To be presented at the International Center for Heat and Mass Transfer Seminar on "Heat and Mass Transfer in Metallurgical Systems," Dubrovnik, Yugoslavia, September 3-7, 1979

MAGNETIC FIELDS, CURRENT DENSITIES, MELT VELOCITIES AND CURRENT EFFICIENCIES IN HALL-HEROULT CELLS - COMPUTATIONS AND COMPARISON WITH MEASUREMENTS

J. W. Evans, Y. Zundelevich,
E. D. Tarapore, and D. Sharma

March 1979

Prepared for the U. S. Department of Energy
under Contract W-7405-ENG-48

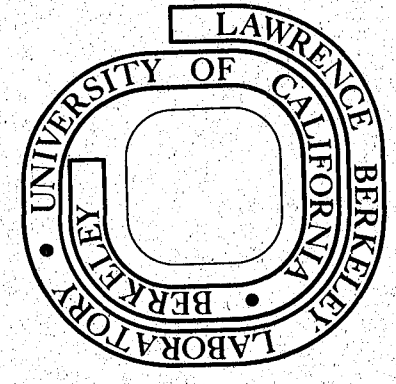

Lawrence Berkeley Laboratory Report LBL-8519

"MAGNETIC FIELDS, CURRENT DENSITIES, MELT VELOCITIES AND CURRENT EFFICIENCIES IN HALL-HÉROULT CELLS - COMPUTATIONS AND COMPARISON WITH MEASUREMENTS"

J. W. Evans (Principal Investigator, Molecular and Materials Research Division, LBL, and Department of Materials Science and Mineral Engineering, University of California, Berkeley, California 94720)

Y. Zundelevich (Molecular and Materials Research Division, LBL)

E. D. Tarapore (Kaiser Aluminum & Chemical Corporation, Permanente, California)

and

D. Sharma (Dames and Moore, Denver, Colorado)

ABSTRACT

The magnetic fields, current densities, metal and electrolyte velocities and current efficiencies within the Hall-Heroult cells used to produce aluminum have been predicted from first principles. The computation of current densities was carried out by solving Ohms law enabling the calculation of magnetic field vectors from the Biot-Savart law. The cross product of the current densities and magnetic fields then yielded the electromagnetic stirring forces acting on the molten metal and electrolyte. By employing a turbulence model and the time averaged Navier-Stokes equations, velocities within these two liquids could be calculated. Following this the mass flux of aluminum from the aluminum-electrolyte interface could be calculated using an equation due to Levich and subsequently the current efficiency predicted. Predicted field strengths and metal velocities within a 185 kiloamp cell were in approximate agreement with measured values.

INTRODUCTION

Almost all the aluminum manufactured in the U. S. is produced in a Hall-Héroult cell in which aluminum oxide, dissolved in a molten cryolite electrolyte, is electrolytically reduced to metal. Approximately 100 billion KWH per year of electrical energy are consumed in this operation and there is, therefore, considerable incentive for improving the performance of the cell.

Part of a cell is shown in cross section in Fig. 1. The molten cryolite is seen to be floating on a pool of molten aluminum. Dipping into the cryolite is a carbon anode and the surface of the molten metal forms the cathode at which the metal is generated. The anode reaction is the generation of carbon dioxide. Cell performance is adversely affected by electromagnetic stirring forces within the molten cryolite and aluminum. A typical modern cell would have a current of 100-200 kiloamps flowing in a predominantly downward direction from anode to cathode. This current and currents flowing in adjacent cell components generate strong magnetic fields, of the order of 100 gauss acting predominantly in the horizontal direction. The interaction of these currents and fields causes a circulation of both cryolite and metal with velocities in the region of 10 cm/sec. Deterioration of the carbon cell lining is promoted by this circulation which also has the effect of reducing the current efficiency of the cell. This reduction in current efficiency arises from the fact that the metallic aluminum generated in

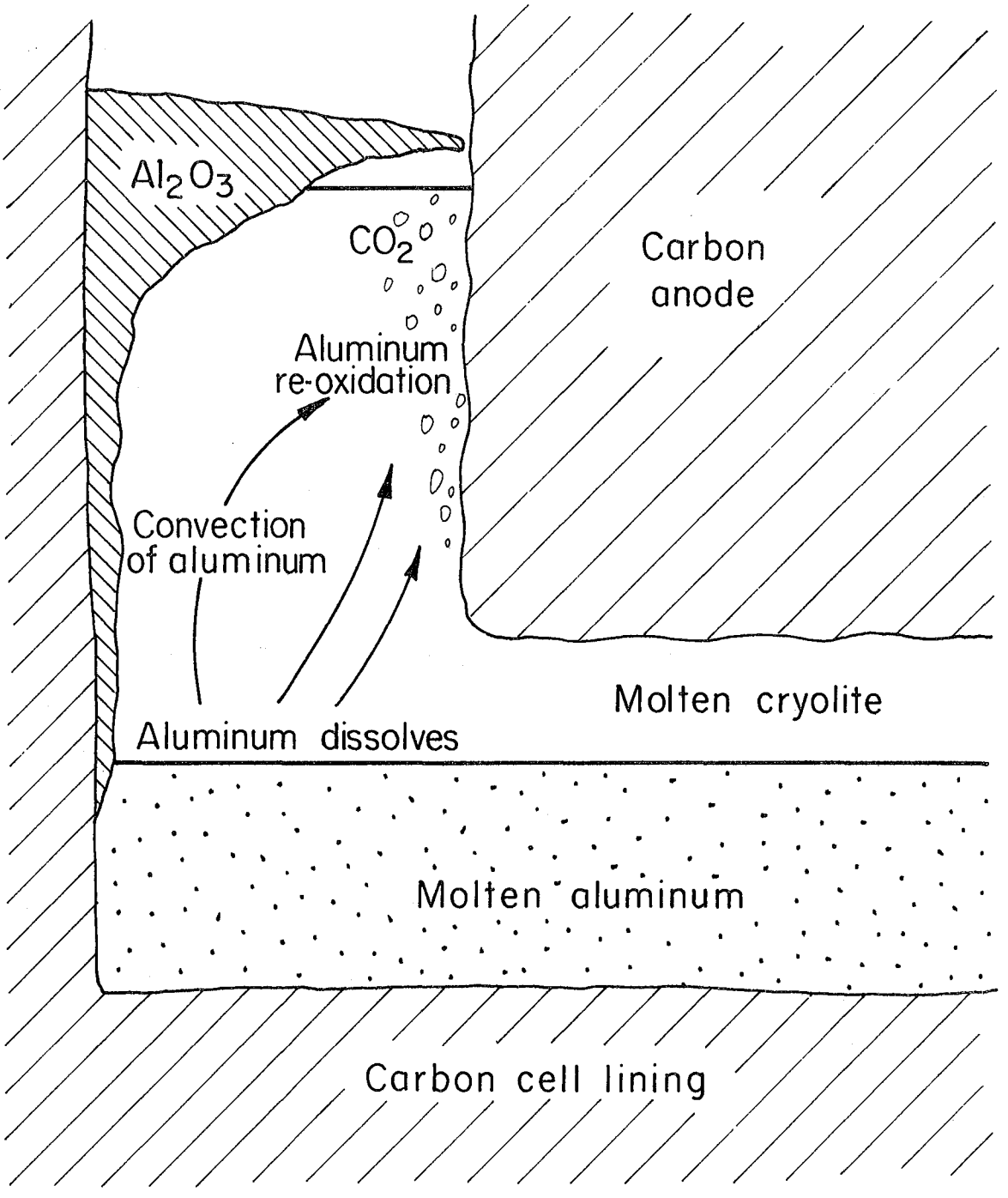

XBL 784-8016

Fig. 1. Transport and re-oxidation of part of aluminum product in the Hall-Heroult cell.

the cell has a small solubility in molten cryolite. This dissolved aluminum is transported to the anode region where it is re-oxidized by carbon dioxide bubbles (1). This transport and re-oxidation of product, illustrated in Fig. 1, results in a loss of current efficiency, which in a typical cell is 85-95%. The transport of the dissolved aluminum is promoted by the turbulence within the cryolite caused by the electromagnetic stirring. This investigation has the objective of predicting the electromagnetic stirring and current efficiency from first principles and thereby providing a means for developing cell designs or operating procedures with higher current efficiences.

The task is threefold. First the currents and magnetic fields must be calculated as a function of position in the cell, yielding the electromagnetic force distribution. Secondly, the turbulent fluid flow equations must be solved with this force distribution to yield velocities and turbulence levels in the cell. Finally the rate of transport of aluminum to the anodes and the current efficiency can be calculated.

COMPUTATION OF CURRENTS AND MAGNETIC FIELDS

The current distribution within the cell was calculated by the application of Ohm's law:

$$\hat{J} = -\sigma \nabla E \qquad (1)$$

where

$\hat{J}$ is the current density vector at any point in the cell

σ the electrical conductivity

and ∇E the potential gradient at that point.

Since current is conserved within the cell

$$\nabla \cdot \hat{J} = 0 \qquad (2)$$

and consequently

$$\nabla \cdot \sigma \nabla E = 0 \qquad (3)$$

It should be recognized that σ will be different in different regions of the cell and that equations (1) - (3) are being used to describe both ionic conduction in the molten electrolyte and electronic conduction in the carbon lining, collector bars, metal pool, etc. A discontinuity in potential occurs at the anode/electrolyte interface and at the electrolyte/metal interface due to the electrolytic reactions taking place at these points. The magnitude of these discontinuities (henceforth the electrochemical potential drop) are known (2). The potential, E, in equations (1) and (3) is therefore defined as the potential with respect to the potential of the collector bar end in the carbon lining, metal pool or collector bar. In the cryolite the potential is defined as the potential with respect to the collector bar end, less the potential difference required to drive the electrochemical reaction at the metal-electrolyte interface. In this way the potential E will be continuous throughout the cell.

A rigorous solution of equation (1) would be a three dimensional one with allowance made for a flow of current in the long horizontal dimension (x direction, see Fig. 2) of the cell. In fact, currents in this direction are usually small compared to horizontal current running in the short cell dimension (y direction) and to the (even greater) currents running in a vertical direction (z direction). Consequently a considerable saving in computer time can be realized by solving the equations in two dimensions (z and y). Additional savings in computer time were realized by exploiting the symmetry of the cell, i.e., the midplane y = constant was assumed to be a

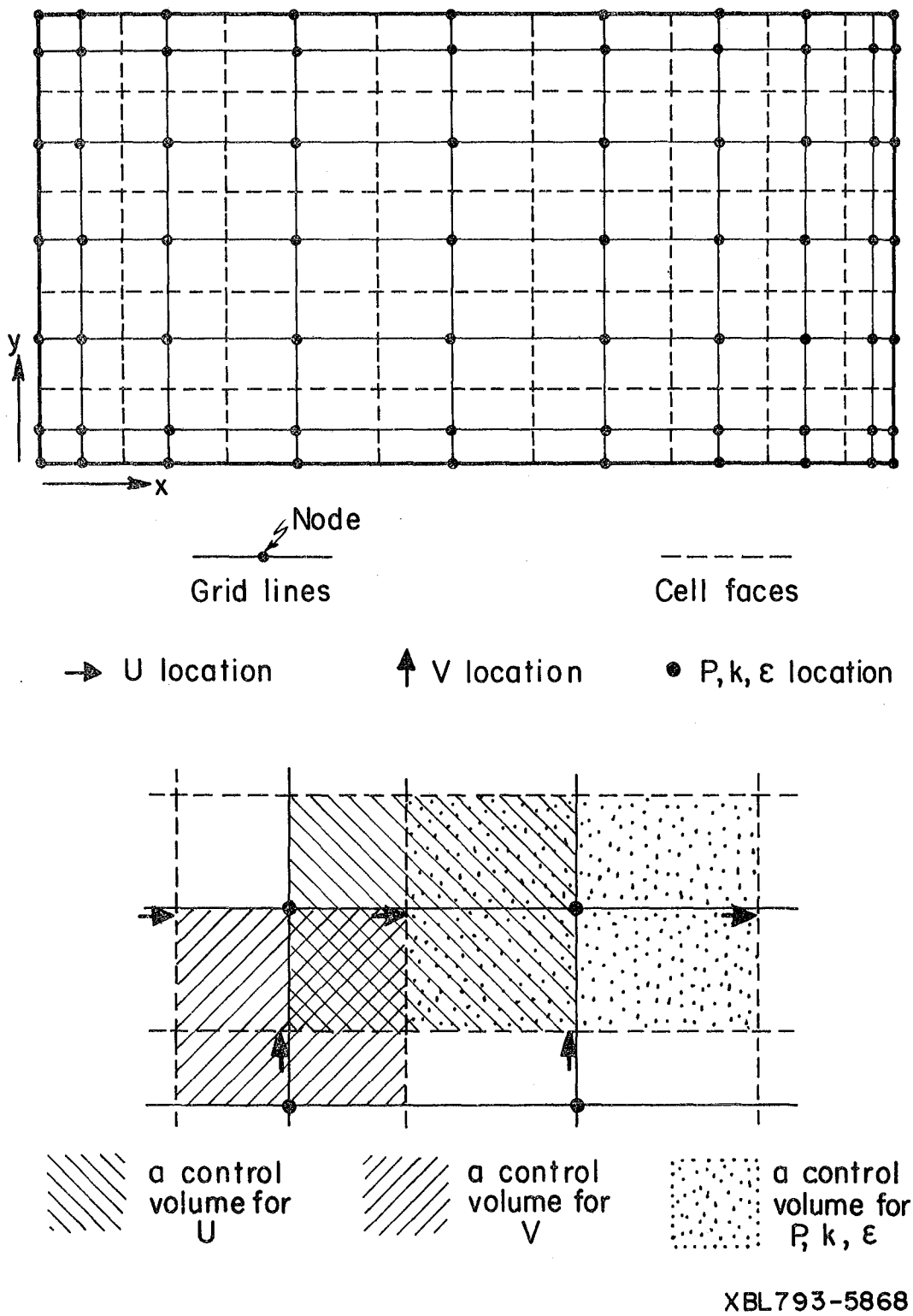

Fig. 2. Finite difference grid employed in melt flow calculations.

surface across which current did not flow. Further boundary conditions employed in the calculation were ones of zero value for E at the ends of the collector bars (by definition) and a value for E equal to the total cell voltage drop less voltage drops for electrochemical reactions at the electrolyte-anode interface. Finally the top surface of the electrolyte and the interface between the carbon cell lining and the refractory (which lies between the carbon and the steel shell) were assumed to be insulating (zero gradient of E normal to the interface). The numerical technique employed in the computations was a finite element procedure of 747 nodes.

The current density distribution having been determined within the cell, the magnetic field strength and direction at any point can be determined by application of the Biot-Savart law in integral form:

$$\hat{H} = \iiint \hat{J} \times \frac{(\hat{r} - \hat{r}')}{|\hat{r} - \hat{r}'|^3} \, dx'dy'dz' \qquad (4)$$

where $(\hat{r}-\hat{r}')$ is the radius vector from the point $(\hat{r})$ at which the field strength vector $\hat{H}$ is to be determined to a point $(\hat{r}')$ at which the current density is $\hat{J}$. The integration is over all volume elements in and around the cell. Strictly equation (4) cannot be applied to the calculation of the magnetic field contribution for current carrying elements outside the cell (ring bus, etc.). This is because the inside of the cell is at least partly shielded by the steel shell. This is accounted for by use of an attenuation factor for contributions from the ring bus, as suggested by Robl (3). It should be noted that while the solution of equation (3) was two dimensional, the integration on the right hand side of equation (4) was carried out (numerically) over three dimensions.

The current densities and magnetic fields having been determined at points within the cell, the electromagnetic stirring forces are readily calculated from

$$\hat{F} = \hat{J} \times \hat{H} \tag{5}$$

COMPUTATION OF ELECTROLYTE AND METAL VELOCITIES

In the aluminum cell the electrolyte and metal move under the influence of three forces. These forces are the electromagnetic stirring force (presumed to be dominant in this study), bouyancy forces due to temperature and concentration gradients, and bouyancy due to the presence of gas bubbles in the electrolyte adjacent to the anode. Only the first kind of force is taken into account here. Since the predominant direction of current flow is vertical, the predominant magnetic field direction is a horizontal one and the predominant electromagnetic stirring force is horizontal (perpendicular to the direction of the predominant magnetic field). Consequently the most significant effect of the electromagnetic field is the stirring of the metal and electrolyte in a horizontal direction. In this study it was therefore assumed that vertical velocity components could be neglected, vertical convection of momentum was thereby treated as negligible and it was also assumed that diffusive (viscous) transport of momentum in a vertical direction was negligible.

As a consequence of these assumptions the time averaged Navier Stokes equations become:

$$\rho U \frac{\partial U}{\partial x} + \rho V \frac{\partial U}{\partial y} = - \frac{\partial P}{\partial x} + \frac{\partial}{\partial x}\left(\mu_e \frac{\partial U}{\partial x}\right) + \frac{\partial}{\partial y}\left(\mu_e \frac{\partial U}{\partial y}\right) + \rho F_x \tag{6}$$

$$\rho U \frac{\partial V}{\partial x} + \rho V \frac{\partial V}{\partial y} = - \frac{\partial P}{\partial x} + \frac{\partial}{\partial x}\left(\mu_e \frac{\partial V}{\partial x}\right) + \frac{\partial}{\partial y}\left(\mu_e \frac{\partial V}{\partial y}\right) + \rho F_y \qquad (7)$$

where

U and V are the time averaged horizontal velocity components of the electrolyte (or molten metal) in the x and y direction respectively

ρ is the density of the electrolyte (or molten metal)

P is the pressure in the electrolyte (or molten metal)

and μ_e is an effective viscosity.

These two equations must be solved in conjunction with the equation of continuity:

$$\frac{\partial V}{\partial x} + \frac{\partial U}{\partial y} = 0 \qquad (8)$$

The effective viscosity appearing in equations (6) and (7) is the sum of the ordinary (laminar) viscosity and a turbulent viscosity introduced to account for the transport of momentum by Reynolds stresses, i.e.,

$$\mu_e = \mu_l + \mu_t \qquad (9)$$

The turbulent contribution to the viscosity, μ_t, was calculated using the k-ε model for turbulence developed by Spalding, Launder and coworkers (4). In this turbulence model μ_t is given by

$$\mu_t = 0.09 \frac{\rho k^2}{\varepsilon} \qquad (10)$$

where

k is the turbulence kinetic energy per unit mass of electrolyte (or metal)

and ε is the turbulence kinetic energy dissipation rate per unit mass.

These two turbulence quantities are obtained from two additional transport equations:

$$U \frac{\partial k}{\partial x} + V \frac{\partial k}{\partial y} = \frac{1}{\rho} \frac{\partial}{\partial x} \left[\frac{\mu_t}{\sigma_k} \frac{\partial k}{\partial x} \right] + \frac{1}{\rho} \frac{\partial}{\partial y} \left[\frac{\mu_t}{\sigma_k} \frac{\partial k}{\partial y} \right]$$

$$+ \frac{\mu_t}{\rho} \left[\left(\frac{\partial U}{\partial y} + \frac{\partial V}{\partial x} \right)^2 + 2 \left(\frac{\partial U}{\partial x} \right)^2 + 2 \left(\frac{\partial V}{\partial y} \right)^2 \right] - \varepsilon \qquad (11)$$

$$U \frac{\partial \varepsilon}{\partial x} + V \frac{\partial \varepsilon}{\partial y} = \frac{1}{\rho} \left[\frac{\mu_t}{\sigma_\varepsilon} \frac{\partial \varepsilon}{\partial x} \right] + \frac{1}{\rho} \frac{\partial}{\partial y} \left[\frac{\mu_t}{\sigma_\varepsilon} \frac{\partial \varepsilon}{\partial y} \right]$$

$$+ C_1 \frac{\mu_t}{\rho} \frac{\varepsilon}{k} \left[\left(\frac{\partial U}{\partial y} + \frac{\partial V}{\partial x} \right)^2 + 2 \left(\frac{\partial U}{\partial x} \right)^2 + 2 \left(\frac{\partial V}{\partial y} \right)^2 \right] - C_2 \frac{\varepsilon^2}{k} \qquad (12)$$

where

$C_1 = 1.44$

$C_2 = 1.92$

$\sigma_k = 1.0$

$\sigma_\varepsilon = 1.3$

It should be noted that the computations have ignored any effect which the magnetic field may have had on the turbulence. Also ignored are any oscillations of the electrolyte-metal interface.

The five differential equations (6)-(8), (11) and (12) were solved simultaneously using a computer program developed by Sharma (5). The algorithm employed was a finite difference procedure with the equations in the form of "primative variables" (U, V and P rather than stream function and vorticity).

A "staggered" finite difference grid was employed wherein the scalar variables (P, k and ε) and the velocity components are computed at locations which are staggered with respect to each other. Grid nodes, representing the intersection of orthogonal (but unequally spaced) grid lines are selected to lie at the geometric centers of associated small control volumes (see Fig. 2). All scalar variables are computed at each grid node. The U velocities are computed at the intersection of the grid lines running in the x direction with the faces of the control volumes parallel to the y axis. The V velocities are computed at the intersection of the y direction grid lines with the faces of the control volumes parallel to the x axis. It should be noted that, in general, the points at which the velocity components are determined will not lie halfway between grid nodes.

The differencing procedure was an integrated hybrid difference scheme. In developing finite difference forms of the differential equations a choice is to be made between upstream and central differences. The latter is more precise but entails needless precision and instability at high values of the ratio of convective to diffusive fluxes (Peclet number). Instead of employing upstream or central differencing throughout the computation, the hybrid procedure permits an automatic local selection of upstream or central differencing. The magnitude of the local Peclet number is used as the criterion for the selection.

Boundary conditions on the velocity components were obtained by the "wall function" method described by Launder and Spalding (4). Boundary conditions on k and ε at the walls were supplied implicitly. The method adopted was based upon the presumption that a wall parallel steady boundary-layer regime persists in the immediate vicinity of the wall. Accordingly it was sufficient to account for boundary layer contributions to the balance

of k and ε ; and in this way the explicit setting of boundary conditions at the wall surface itself was avoided. Specifically, provision was made to account for the generation of turbulence energy by virtue of wall-dominated shear. This provision was based upon the semi-logarithmic law of the wall (4). The diffusion of k at the wall itself, which requires the value of k at the wall itself, was neglected. For the energy dissipation rate, ε , the near-wall value was fixed from a knowledge of k and the linearity of the turbulence length scale in the vicinity of the wall, thereby eliminating the need to supply the values or flux of ε at the wall boundaries.

Transformation of equations (6)-(8), (11) and (12) into finite difference form is the equivalent of performing a balance on a small control volume such as illustrated in Fig. 2. It is therefore necessary to obtain the transport coefficients at the faces of the control volume, which, in the case of scalar variables, lie midway between grid nodes. It is customary to calculate the transport coefficients at these midway points as the arithmetic mean of the values at adjacent grid nodes. Such a procedure results in erroneous flux computations when the midway point in question lies at an interface between two regions with vastly different transport coefficients (e.g. a wall). It may be shown (5) that a more appropriate value for the transport coefficient at a midway point is the harmonic mean of the values at adjacent grid nodes and such a mean was incorporated in the computations.

The set of finite difference equations was solved iteratively in a line-by-line fashion by repeated application of the well known tri-diagonal matrix algorithm (TDMA) (6). In this procedure the finite difference forms of equations (6), (7), (11) and (12) are solved, one at a time, along a line of

grid nodes. This line is then swept through the mesh in a direction perpendicular to itself. The sweep direction is alternated between the y direction and the x direction as is the sense of the sweep (left to right on one sweep in the x direction, right to left on the next sweep in the x direction, etc.). Since, typically, the values of U and V are only weakly dependent on μ_e the equations (11) and (12) were not solved on every iteration but rather every few iterations. Values of U and V obtained on each iteration of (6) and (7) will not necessarily satisfy the equation of continuity (8), consequently the values are adjusted to satisfy (8) on each iteration using a procedure described by Sharma (5). In this way, at convergence, a velocity and pressure distribution is obtained which satisfies all three equations (6)-(8). Underrelaxation is employed during the iterations. The grid used had 11 x 19 nodes.

CALCULATION OF MASS TRANSPORT RATES AND OF CURRENT EFFICIENCY

The computation of the velocity components, k and ε throughout the molten electrolyte and metal, described in the previous section, also yields the distribution of the effective viscosity in the two cell liquids. From this last distribution it is possible to calculate the distribution of the eddy (mass) diffusivity throughout the electrolyte by making the usual assumption that the turbulent Schmidt number is close to unity. The turbulent diffusivity calculated in this way averaged 27 cm^2/sec over the region of the electrolyte which is beneath the anodes. This should be compared with a value of 5 cm^2/sec determined experimentally by Berge et al. (11). From the eddy diffusivity, the anode-metal distance and the solubility of the aluminum in the molten cryolite it is then possible to estimate the rate of mass transport of

dissolved aluminum from the metal-electrolyte interface to the anodes where it is reoxidized. Such an estimate yields a rate of mass transport higher than that at which aluminum is being produced in the Kaiser cell.

The explanation for this anomaly is that in the vicinity of the metal-electrolyte interface the turbulent transport of dissolved aluminum (and momentum) is damped by the surface tension at that interface. Consequently, the rate controlling step in the aluminum transport/reoxidation sequence is the transport of aluminum through a concentration boundary layer at the metal-electrolyte interface. Levich (8) has considered mass transport through such surface tension induced boundary layers and derived an equation for the mass flux of dissolved species:

$$j = \left(\frac{D \rho V_t^3}{\sigma_t}\right)^{1/2} C_s \qquad (13)$$

where

j is the mass flux of dissolved species

D the diffusivity of the dissolved species

V_t is the mean fluctuating velocity component outside the boundary layer

C_s is the solute concentration at the interface

σ_t is the interfacial tension

V_t is related to the turbulence kinetic energy by

$$V_t = \sqrt{k} \qquad (14)$$

and consequently equation (13) becomes

$$j = \left(\frac{D \rho C_s^2}{\sigma_t}\right)^{1/2} k^{3/4} \qquad (15)$$

The rate of mass transport from the metal to the anodes was calculated using equation (15). In this calculation the mass transport was assumed to be purely in a vertical direction and to take place only underneath the anodes, i.e., the area available for mass transport was equal to the sum of the anode cross sections in the cell. The value used for k was obtained by averaging, over the electrolyte, the k distribution obtained in the velocity calculations. C_s was assumed to be the equilibrium value and this value and σ_t were obtained from the literature (7). The current efficiency was then obtained from

$$\text{Current efficiency } (\%) = 100 \quad \left(1 - \frac{\text{Mass transport rate of Al to anodes}}{\text{Al production rate expected from Faraday's law}}\right) \qquad (16)$$

RESULTS OF CALCULATIONS AND DISCUSSION

Fig. 3 depicts the isopotential lines in a 185 kiloamp Kaiser cell computed by the finite element technique described above, while Fig. 4 shows the computed horizontal components of the magnetic field at the top of the electrolyte pool, together with those measured on the cell using a Hall effect probe. In view of the assumptions entailed in the model, the agreement between measured and calculated values appears reasonable.

In Fig. 5 the computed and measured values of metal velocity within the molten metal pool are compared. Metal velocity measurements were determined by measuring the rate of dissolution of iron rods in the aluminum, as described by Johnson (9). The magnitudes of the computed velocities within the metal are comparable with the magnitudes of the measured velocities. However the computed velocity directions show poor agreement with measured

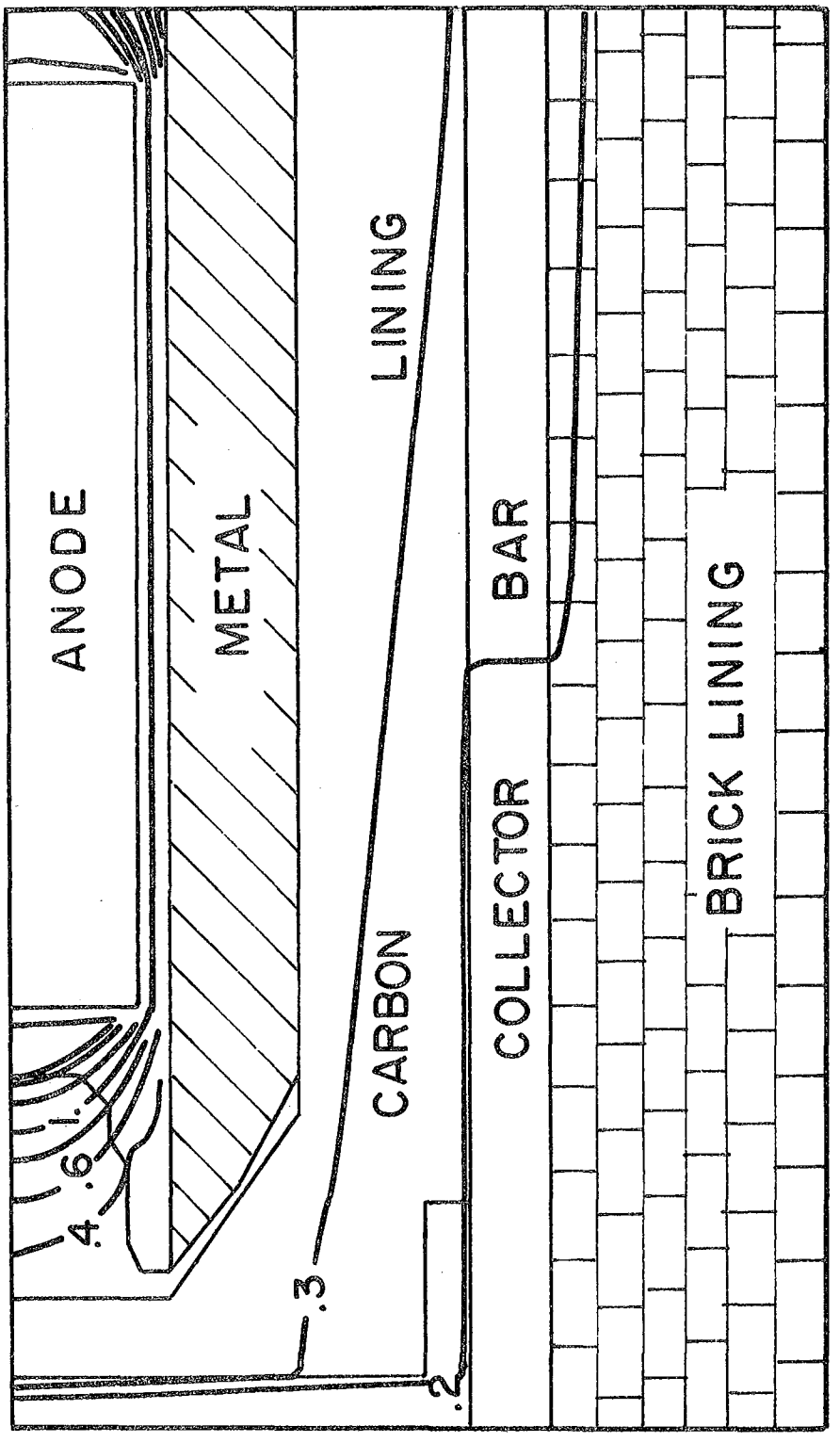

XBL7811-6172

Fig. 3. Isopotential lines (volts) in a 185 kiloamp Kaiser cell computed by the finite element technique.

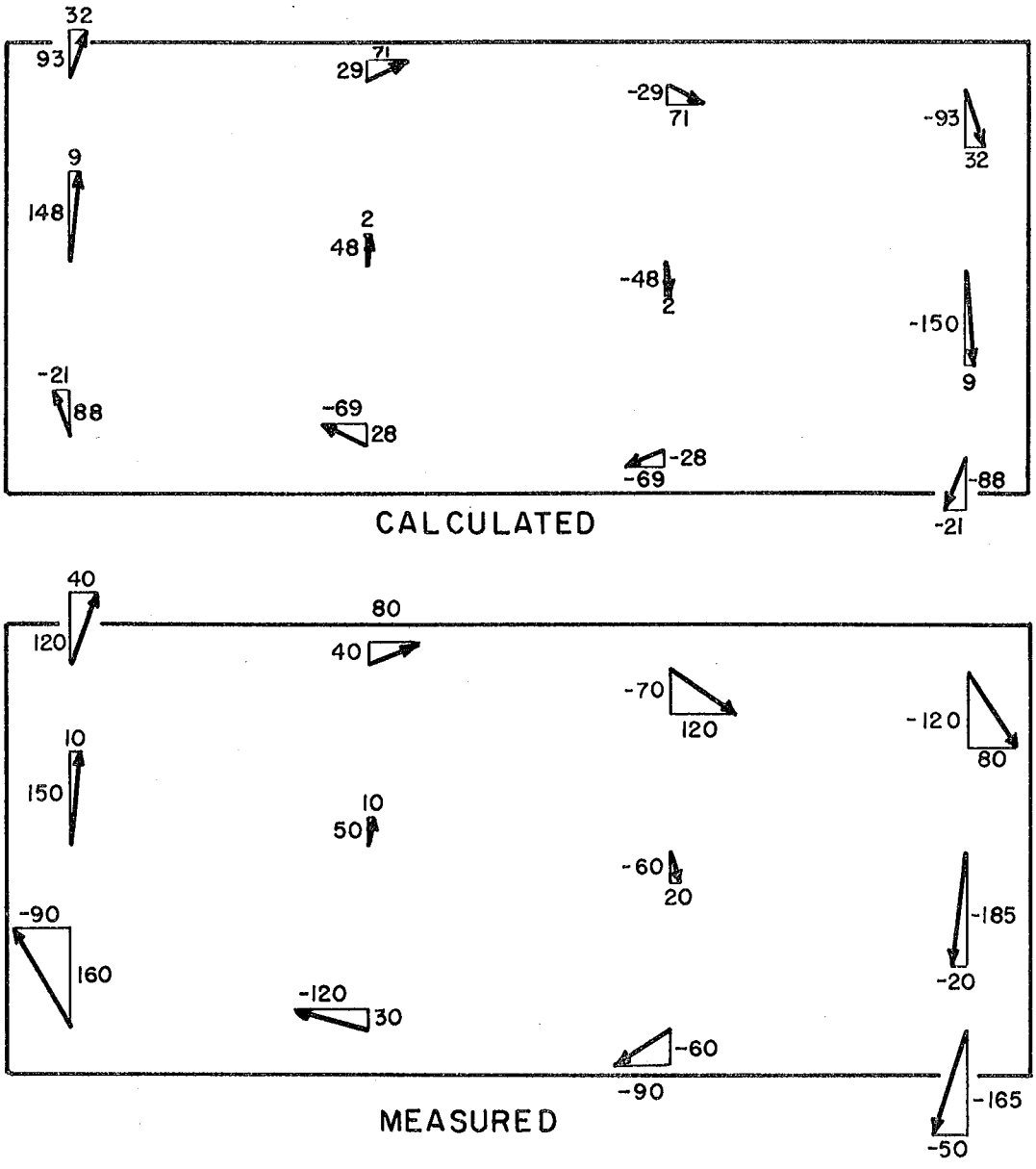

Fig. 4. Computed and measured components of the horizontal magnetic field components (gauss) within the electrolyte of the 185 kiloamp cell.

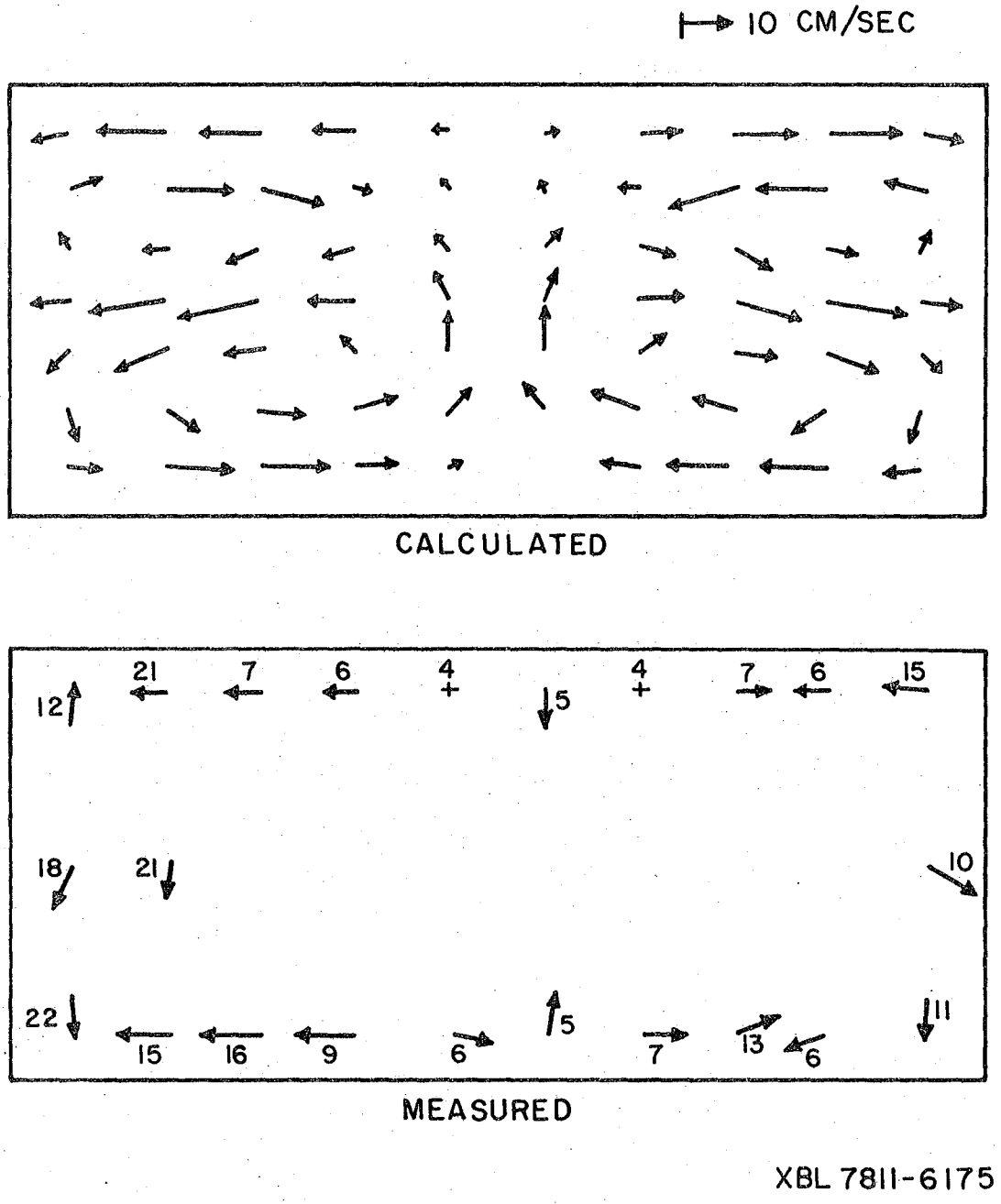

Fig. 5. Computed and measured velocities within the molten aluminum of the 185 kiloamp cell.

directions in some regions of the cell (e.g., lower left hand edge of each drawing).

Computed velocities in the molten cryolite electrolyte below the level of the bottoms of the anodes are presented in Fig. 6. The computed velocities are seen to reach higher values than those computed for the molten metal. Presently there are no data on electrolyte velocities within the Kaiser cell to enable a comparison of computed and measured velocities. Fig. 7 gives the values of the turbulence kinetic energy (cm^2/sec) computed for various points within the molten salt electrolyte. Again there are no experimental data for comparison with these calculated values.

Fig. 8 shows the calculated current efficiency in the Kaiser cell as a function of cell current. The prediction of a current efficiency close to 100% at low currents is unrealistic; the model does not take into account other stirring effects in the cell (circulation arising from bouyancy due to gas bubbles or density gradients) which may dominate at low cell currents. It should be noted that the curve is unrealistic in another respect since it assumes that the geometry of the cell is unchanged on altering the cell current. Practically, such an alteration cannot be realized; alteration of the current changes the cell heat balance which alters the thickness of the solidified alumina around the cell wall or forces changes in the anode-metal distance. The current efficiency of the Kaiser cells is proprietary information but Grotheim and coworkers (10) have reported values mostly in the range 80-90% for an older cell with Soderberg (self baking) anodes.

Equation (15) predicts an increase in mass flux (lower current efficiency) as the electrolyte-metal interfacial tension is lowered. This is consistent

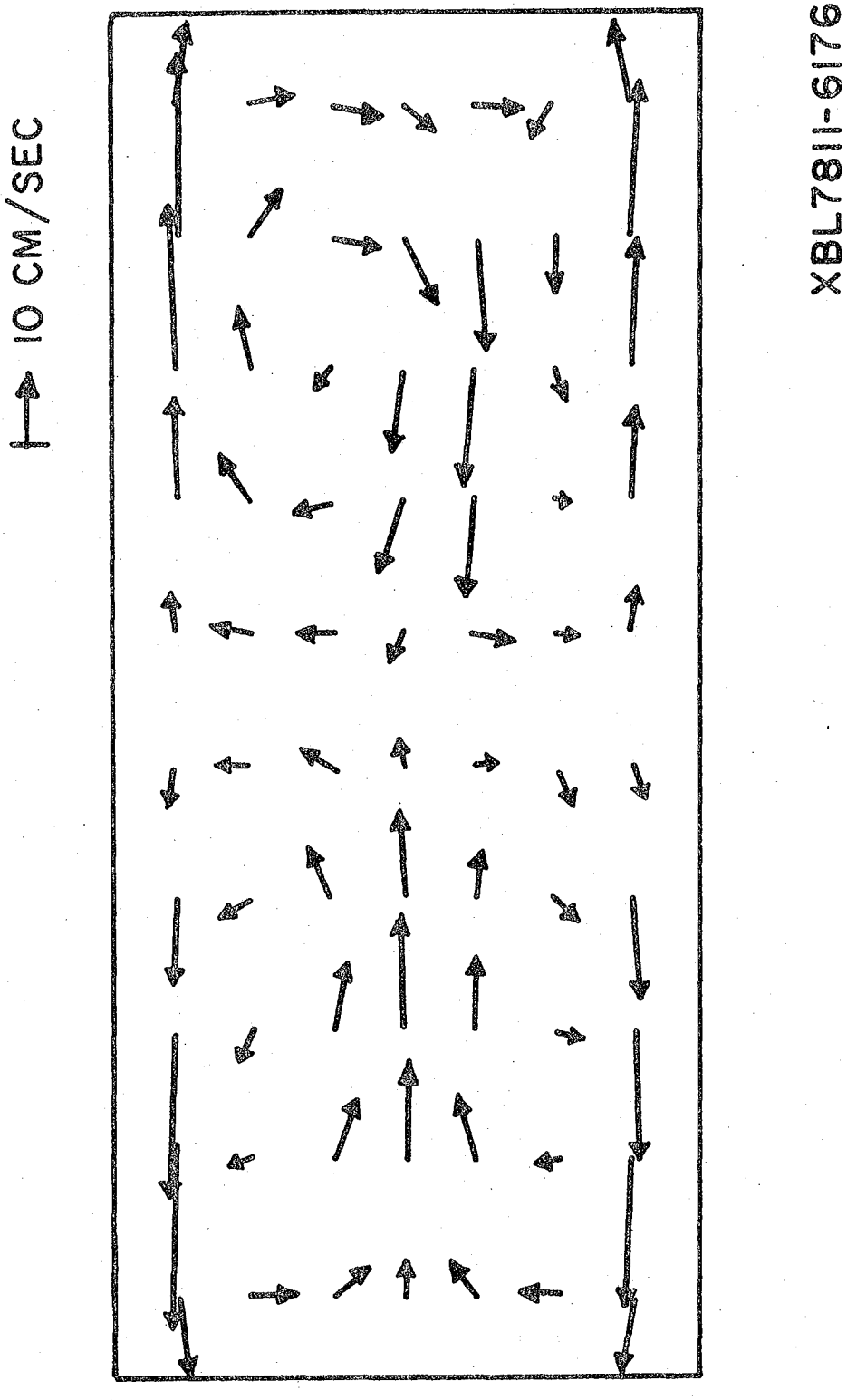

Fig. 6. Computed velocities within the electrolyte of the 185 kiloamp cell.

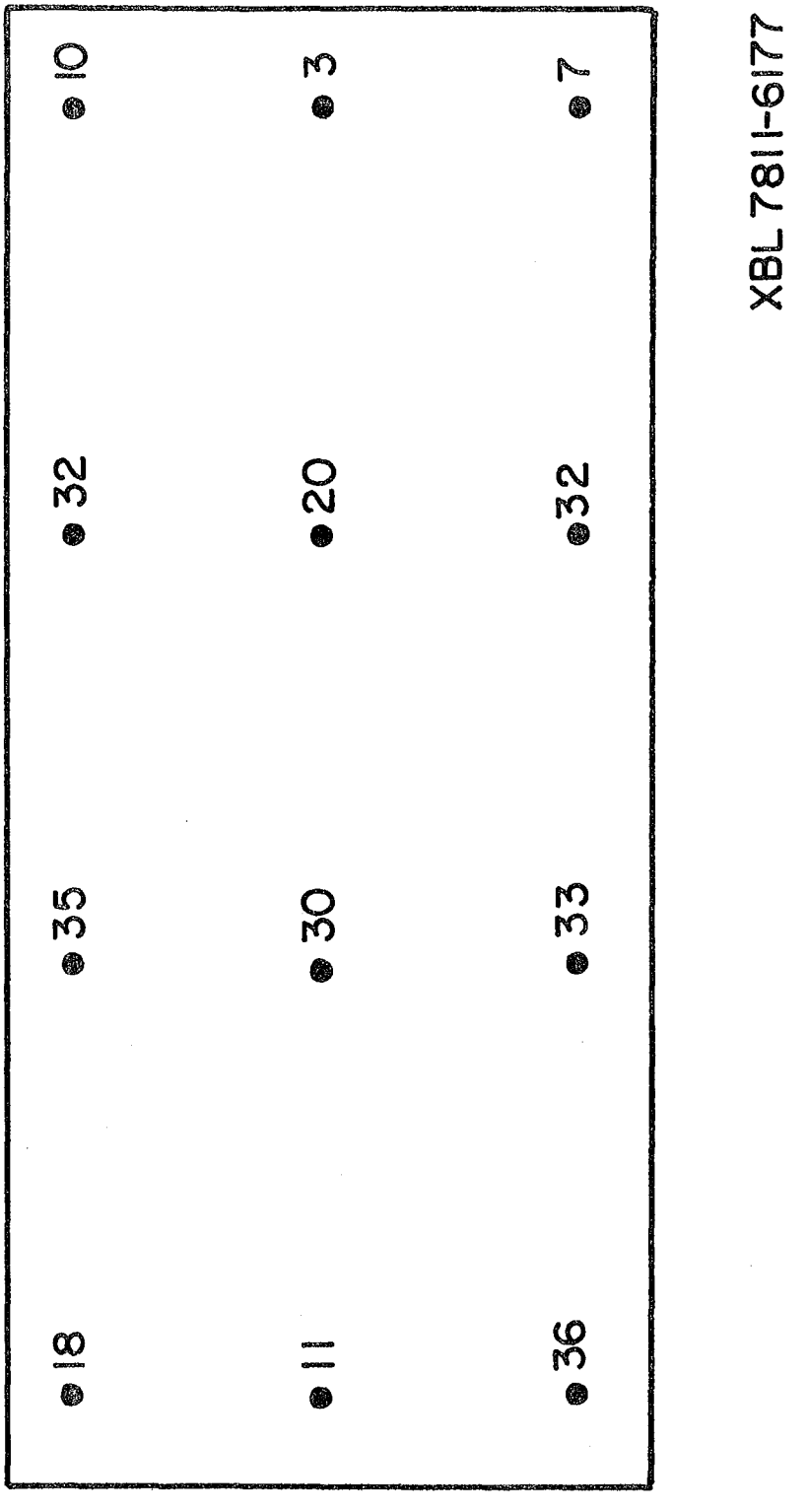

Fig. 7. Computed turbulence kinetic energies (cm^2/sec^2) within the electrolyte of the 185 kiloamp cell.

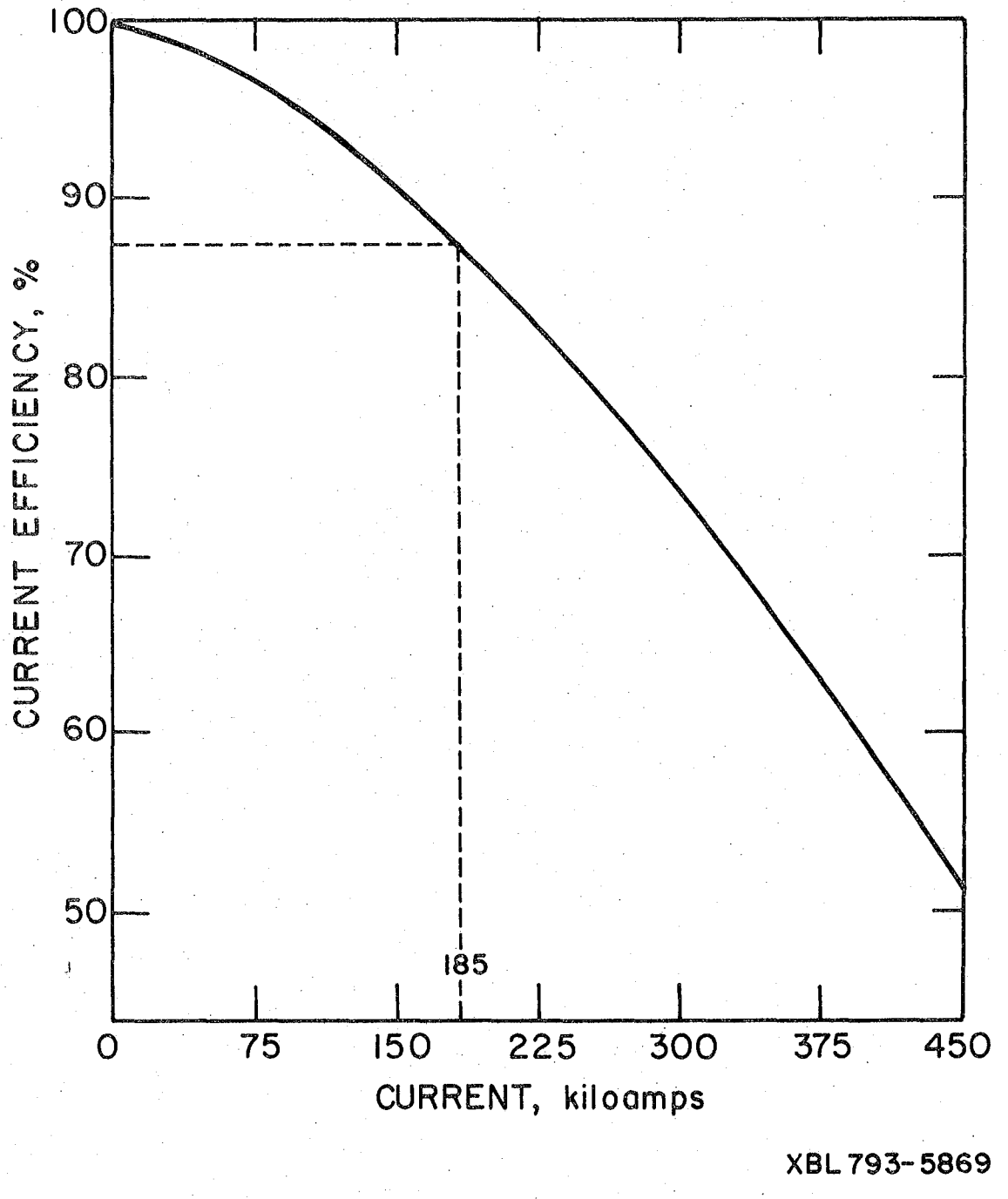

Fig. 8. Computed current efficiency for the 185 kiloamp cell as a function of cell current.

with the results of Belyaev and coworkers and other investigators as reported by Grotheim (7). These investigators observed that the rate of aluminum transport at the molten metal-cryolite interface was increased by changes in metal or cryolite which reduced interfacial tension.

CONCLUDING REMARKS

The mathematical model described in this paper must be regarded as a preliminary one subject to further refinement and testing. However, the results of initial computations are encouraging. It is suggested that with modest additional effort the model will become a useful tool for the improvement of the aluminum cell by changing parameters under the control of the designer or operator.

ACKNOWLEDGEMENT

The part of this research performed at Lawrence Berkeley Laboratory (LBL) was supported by the Division of Solar, Geothermal, Electric and Storage Systems, Office of the Assistant Secretary of Energy Technology, U.S. Department of Energy under contract number W-7405-Eng-48.

LIST OF SYMBOLS

C_1, C_2	constants in the k-ε turbulence model
D	diffusivity of solute
C_s	concentration of solute at interface
E	electric potential
$\hat{F}$	electromagnetic force vector
$\hat{H}$	magnetic field vector
$\hat{J}$	current density vector
j	mass flux of solute at interface
k	turbulence kinetic energy
P	pressure
r, r'	vectors indicating position in melt
U	x direction velocity component
V	y direction velocity component
V_t	fluctuating part of turbulent velocity
x	long horizontal direction in cell
y	short horizontal direction in cell
ε	turbulence kinetic energy dissipation rate
μ_l, μ_t, μ_e	laminar, turbulent and effective viscosity
ρ	density
σ	electric conductivity
σ_k, σ_e	turbulent Prandtl number for k, ε
σ_t	interfacial tension

REFERENCES

(1) R. F. Robl, W. E. Haupin and D. Sharma, paper no. A77-35 presented at the AIME annual meeting, Atlanta, Georgia, 1977, available from the Metallurgical Society of AIME, New York, N. Y.

(2) JANAF Thermochemical Tables, 2nd ed., U.S. Dept. of Commerce, Nat. Bureau of Standards, Washington, 1971.

(3) R. F. Robl, "Influence by Steel Shell on Magnetic Fields within Hall-Héroult Cells" in "Light Metals 1978, Vol. I", pp. 1-14, The Metallurgical Society of AIME, New York, N. Y., 1978.

(4) B. E. Launder and D. B. Spalding, Computer Methods in Applied Mechanics and Engineering, Vol. 3, 269-289 (1974).

(5) D. Sharma, "Details of an Efficient Computational Procedure for the Prediction of Convective Heat, Mass and Momentum Transfers", Report ATG/TN/DN/41, Advanced Technology Group, Dames and Moore, Denver, Colorado.

(6) Dale U. vonRosenberg, "Methods for the Numerical Solution of Partial Differential Equation", Elsevier, New York, N. Y., 1969.

(7) K. Grjotheim et al., "Aluminum Electrolysis, The Chemistry of the Hall-Héroult Process", Aluminum-Verlag GmbH, Dusseldorf, 1977.

(8) V. G. Levich, "Physicochemical Hydrodynamics", pp. 690-698, Prentice-Hall, Inc., Englewood Cliffs, N. J., 1962.

(9) A. F. Johnson, "Metal Pad Velocity Measurements in Aluminum Reduction Cells" in "Light Metals 1978, Vol. I", pp. 45-58, The Metallurgical Society of AIME, New York, N. Y., 1978.

(10) K. Grjotheim et al., Metallurgical Transactions,Vol. 2, 199-204 (1971).

(11) B. Berge et al., Metallurgical Transactions, Vol. 4, 1945-1952 (1973).

TECHNICAL INFORMATION DEPARTMENT
LAWRENCE BERKELEY LABORATORY
UNIVERSITY OF CALIFORNIA
BERKELEY, CALIFORNIA 94720